



Effect of TiO₂ and Synthesis Strategies on Formate Oxidation: Electrochemical and Fuel Cell Approaches

Vitória Pistori Guimarães¹ · Júlio Nandinha² · Luiz Otávio Orzari^{3,4} · Orlando Fatibello-Filho⁵ · Almir Oliveira Neto² · Bruno Campos Janegitz³ · Fernando Campanhã Vicentini¹ · Mônica Helena Marcon Teixeira Assumpção¹

Accepted: 24 October 2022 / Published online: 3 November 2022

© The Author(s), under exclusive licence to Springer Science+Business Media, LLC, part of Springer Nature 2022

Abstract

Direct formate fuel cells have gained increasing attention since formate can be obtained by CO₂ reduction, being shown as a renewable power source. This paper reports the use of Pd nanoparticles supported on physical mixtures of Vulcan carbon and TiO₂ in different ratios and different Pd reduction methodologies. The materials were prepared using sodium borohydride as a reducing agent and analyzed toward formate oxidation in alkaline media. The prepared electrocatalysts showed peaks of Pd face-centered cubic and TiO₂ anatase and rutile phases and an average particle size between 3.7 and 7.9 nm. Experiments considering formate electro-oxidation (voltammetry and chronoamperometry) showed that the presence of TiO₂ is favorably using both synthesis methodologies while single cells revealed Pd nanoparticles supported on physical mixtures of carbon and TiO₂, in the proportion of 75:25 as the most efficient, which was explained by the carbon high electrical conductivity and small quantities of TiO₂ working as co-catalyst.

Keywords Pd nanoparticles · TiO₂ · Formate electro-oxidation · Direct formate fuel cell

Introduction

According to Goldemberg [1], the marvelous machine produced by the evolutionary process—the human body—is driven by water, oxygen, and by food which supplies the modest energy needed for a human to go around and produce knowledge likewise the machines that drive our modern society. However, these machines consume huge amounts of energy. As stated by International Energy Agency (IEA), the energy consumption of the world economy increased

around twice from 1975 to 2015 [2] and estimations reveal that energy utilization will increase by around 30% between 2015 and 2040, worldwide [3].

Most energy consumption comes from fossil fuels such as coal, oil, and natural gas. About 80% of the energy consumed in the world is supplied by this type of fuel, which is worrying since it has been recognized that human civilization is over-exploiting the planet's resources faster than they are being renewed [4–6]. Additionally, although fossil fuels are still the cheapest energy source, it is non-renewable and reserves will deplete and run out, eventually. Moreover, burning this energy source increases CO₂ emissions and consequently contributes to climate change, which emerged as a major concern for humanity over the last two decades [7, 8].

With this scenario, the power industry seeks to increase the production of renewable energy production to meet energy demands with more sustainable development [5]. In this context, many effective approaches can be used to reduce the influence of CO₂ emissions and an example is the fuel cell, an electrochemical device that combines chemical fuels and electrocatalysts to produce electricity cleanly [6, 9].

✉ Mônica Helena Marcon Teixeira Assumpção
monicahelena@ufscar.br

¹ Federal University of São Carlos (UFSCar), Lagoa do Sino Campus, 18290-000 Buri, SP, Brazil

² Nuclear and Energy Research Institute (IPEN/CNEN), University City, 05508-000 São Paulo, SP, Brazil

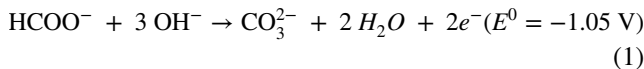
³ Department of Nature Sciences, Mathematics and Education, Federal University of São Carlos, 13600-970 Araras, SP, Brazil

⁴ Department of Physics, Chemistry, and Mathematics, Federal University of São Carlos, 18052-780 Sorocaba, SP, Brazil

⁵ Department of Chemistry, Federal University of São Carlos (UFSCar), 13560-970 São Carlos, SP, Brazil

Among the fuel cell types, the Direct Liquid Fuel Cell (DLFC) is under intense study due to its advantages over hydrogen-based ones, which need to store the explosive fuel under high pressure, while also being flammable and presenting transportation issues; besides, it shows simple structural design [10–14]. In DLFC, the liquid fuel is oxidized at the anode, and the oxygen gas is reduced at the cathode. The charged ions pass through the electrolyte and the electrons travel through an external circuit. Many liquid fuels have been used in DLFC, but alcohols (such as ethanol and methanol) are the most common [10, 14].

However, formate has been emerging as a promising fuel since it is non-flammable, non-toxic, relatively low cost, and renewable, as it can be obtained from the electrochemical reduction of CO₂ [15, 16]. Thus, formate also gives a lower theoretical reversible potential (Eq. 1) which combined with the cathode half-reaction (Eq. 2) results in an overall theoretical voltage for the direct formate fuel cell of 1.45 V, a value of 0.24 V and 0.31 V higher than those cells using methanol and ethanol as fuel, respectively [17, 18].



One drawback faced by DLFC is the high cost of electrocatalysts [14, 19, 20]. As reported by An et al., formate oxidation is facile in alkaline media using palladium electrocatalysts [21]; however, it is a most costly material, which hinders the development of fuel cells [22]. Thus, one way to improve the catalyst utilization and decrease the fuel cell cost is by using nanoparticles supported by carbon materials due to their high electrical conductivity. However, carbon is susceptible to corrosion which makes it less favorable for fuel cell applications; therefore, its replacement by a metallic oxide could be extremely important [23, 24].

According to Bandarenka et al. [25], one common factor that controls catalyst performance is the interaction between nanoparticles and supports. Hence, another way to improve the electrocatalysts' efficiency is by developing different supporting materials [10, 26]. Among them, TiO₂ shows good mechanical resistance and stability in oxidative environments, it is non-toxic, and has a relatively low price, characteristics that suggest TiO₂ as alternative support. Furthermore, TiO₂ could show the co-catalytic effect on fuel oxidation [23, 27–29], which is an advantage since according to the Sabatier principle [25, 30], the surface of the active electrocatalyst should be able to activate the reactants and at the same time should not bind the reaction intermediates too strongly to prevent poisoning of the active site.

Considering the use of TiO₂ as a support, it is also important to highlight that theoretical studies showed that spontaneous dissociative H₂O adsorption occurs on the (001) TiO₂

surface, whereas molecular H₂O adsorption is prevalent on the (101) surface. The crystallite shape of anatase (phase of titanium oxide) is a truncated bipyramid, exposing both the (101) and (001) surfaces, then a large quantity of (001) surface planes can be supplied by TiO₂. So, dissociative H₂O adsorption on the (001) anatase surface produces a plentiful Ti–OH surface group, improving the bifunctional mechanism [24, 31].

Although TiO₂ shows low electrical conductivity and surface area [32], when compared to carbon black, it could act as a co-catalyst and also improve the bifunctional mechanism. In this context, in this work, we studied the efficiency of Pd nanoparticles supported on physical mixtures of carbon black and TiO₂, toward formate oxidation, in alkaline media. We also investigated the influence of the TiO₂ introduction in the catalysts by using different synthesis methodologies. In the first one, the Pd was reduced in a physical mixture of carbon and TiO₂, and in the second one, the Pd was reduced firstly in TiO₂, and carbon was inserted after this step. All the prepared electrocatalysts were studied considering not only the electrochemical but also the fuel cell experiments. To the best of our knowledge, this is the first time that the oxidation of formate is studied using Pd on different supports of carbon and TiO₂, regarding also the synthesis strategies.

Experimental

Synthesis of the Catalysts

Pd nanoparticles (PdNPs) were obtained by the borohydride method [33, 34] using Pd(NO₃)₂·2H₂O (Aldrich) as the metal source, Vulcan XC72 (Cabot)+TiO₂ P25 (Degussa) as supports, and sodium borohydride (Aldrich) as reducing agent. The electrocatalysts were prepared in two batches. In the first one, the PdNP was reduced in the physical mixture of carbon (C) + TiO₂, and these electrocatalysts were called Pd/(C + TiO₂). In the second one, the PdNP was firstly reduced in TiO₂, and C was inserted after. These electrocatalysts were called Pd/TiO₂-C. In all prepared materials, the mass proportions of the supports C:TiO₂ were studied in the following mass ratio percentages: 75:25, 50:50, and 25:75. The C:TiO₂ ratio was maintained by weighting different amounts of the materials considering the total mass of support. The metal loading was set to 20 wt%.

Physical Characterizations

To study the morphology of the prepared electrocatalysts, Transmission Electron Microscopy (TEM) was employed by using a JEOL-JEM-2100 electron microscope with a 200 kV voltage at Instituto de Pesquisa Energéticas e Nucleares. The

average size of the nanoparticles was obtained using ImageJ software and the nanoparticle's mean diameter counting procedure was performed over 100 nanoparticles. X-ray diffraction (XRD) patterns were taken by PANalytical X'Pert PRO with CoK α radiation source ($\lambda=0.179$ nm) conducted in the range of $2\theta=20$ to 110° with a step size of 0.05° and scan time of 2 s per step at Laboratório Nacional de Pesquisa em Energia e Materiais (CNPEM) at Campinas—Brazil. For comparison, XRD patterns were converted to CuK α using Bragg law.

Electrochemical Measurements

Electrochemical measurements were carried out in a one-compartment glass cell and three-electrode setup (half-cell): an Ag/AgCl/KCl (3.0 mol L $^{-1}$) was used as a reference electrode; a platinum foil as a counter electrode; and the working electrode was a glassy carbon electrode ($\varnothing=3.0$ mm; geometric area of ~ 7 mm 2) used as the substrate for electrocatalysts films. The catalysts were applied to the glassy carbon electrode (GCE) by adding 5 μ L of a catalyst suspension and dried at room temperature. The catalyst suspension was prepared by sonicating 6 mg of the catalyst powder, 900 μ L of water, 100 μ L of isopropyl alcohol, and 20 μ L of 5% Nafion $^{\circledR}$ solution.

Cyclic Voltammetry (CV) and Chronoamperometry (CA) analyses were conducted in a potentiostat/galvanostat μStat 200 (DropSens) controlled by DropView 1.3 software. The CV curves were recorded at the potential limits of -0.85 V and 0.05 V with a potential scan rate of 10 mV s $^{-1}$ in 2.0 mol L $^{-1}$ potassium hydroxide aqueous solution in the presence and absence of 0.02 mol L $^{-1}$ potassium formate. The CA curves were obtained in the electrolyte composed of KOH and HCOOK at -0.55 V for 1800s. The current densities were normalized to the Pd mass.

The Electrochemical Impedance Spectroscopy (EIS) analyses were performed in a PGSTAT204 potentiostat/galvanostat (Metrohm, Eco-Chemie), in a conventional three-electrode cell, namely: GCE, Platinum, and Ag/AgCl/KCl (3.0 mol L $^{-1}$) respectively as working, auxiliary, and reference electrodes. The tests were carried out in the presence of 1.0 mmol L $^{-1}$ [Fe(CN) $_6$] $^{3/4-}$, in a 0.1 mol L $^{-1}$ KCl medium. The technique was performed with a potential of 0.2 V ($E_{1/2}$ of the system, identified by CV) with sine type wave, amplitude of 10 mV, and frequency ranging from 10^5 to 0.1 Hz.

The dispersion with the electrocatalysts was prepared in the proportion of 12 mg to 1800 μ L of ultra-pure water (resistivity ≥ 18.0 MΩ cm), 200 μ L of isopropyl alcohol, and 40 μ L of Nafion. The dispersion was then ultrasonicated for 30 min, and 6.0 μ L was cast on the GCE surface, with a drying time of 90 min before use.

Fuel Cell Measurements

The polarization curves of a 5 cm 2 single-cell area were recorded using a PGSTAT 302 N potentiostat/galvanostat Autolab. The Membrane Electrode Assemblies (MEA) were prepared as reported previously [35]. The electrocatalyst dispersion prepared using Nafion $^{\circledR}$ solution (5 wt%, Aldrich) was painted over a carbon cloth. The catalytic ink was formulated in a way that Nafion $^{\circledR}$ comprised 35% wt% of the total solids in the ink and this was applied to the carbon cloth. After its preparation, the electrodes were hot-pressed on both sides of a Nafion $^{\circledR}$ 117 membrane at 125 °C for 10 min under a pressure of 247 kgf cm $^{-2}$. Before being used, the membranes were exposed to 6 mol L $^{-1}$ KOH for 24 h. All cathodes and anodes were prepared with 1.0 mg metal cm $^{-2}$ of metal loading. In all experiments, the fuel cell was maintained at 60 °C and the oxygen humidifier at 85 °C with a flow rate of 150 mL min $^{-1}$. The fuel, 1.0 mol L $^{-1}$ HCOONa and 2.0 mol L $^{-1}$ NaOH, was delivered at 1.0 mL min $^{-1}$. A commercial Pt/C (BASF) cathode was used in all experiments.

Results and Discussion

Physical Characterizations

Figure 1 shows the TEM images which evidence more dispersed nanoparticles on Pd/(C + TiO $_2$) batches when compared to Pd/TiO $_2$ -C, although the mean particle sizes are similar. The histograms of all electrocatalysts were prepared to reveal that the mean particle sizes are in the range of 3.7 to 7.9 nm. According to Song et al. [36], the agglomeration of Pd particles can easily occur on TiO $_2$ supports when the Pd is loaded on TiO $_2$ supports, which could make the active surface area lower, reducing the catalytic efficiency.

Figure 2 presents XRD patterns for Pd/(C + TiO $_2$) and Pd/TiO $_2$ -C batches. The diffraction peaks at about 40.0° , 46.6° , 68.1° , and 82.1° are associated with (111), (200), (220) and (311) planes, characteristic of the crystal face of Pd, as already observed before [37] and according to JCPDF# 88–2335. From this figure, it is also possible to observe peaks of the anatase phase of TiO $_2$ at $2\theta=25.3^\circ$, 37.8° , 48.0° , 53.9° , 55.1° , 62.7° , 68.8° , 70.3° , and 75.0° and of rutile phase of TiO $_2$ at $2\theta=27.4^\circ$, 36.1° , 41.2° , and 56.7° , as also observed before [38]. The mean crystallite (estimated using the Scherrer equation) and average nanoparticle sizes are listed in Table 1. No shift was observed at the positions of the Pd diffraction peaks in the Pd/(C + TiO $_2$) and Pd/TiO $_2$ -C catalysts when compared to Pd/C, showing that the addition of TiO $_2$ does not affect the crystalline lattice of Pd [18].

Fig. 1 TEM images of the two batches of prepared materials: Pd/(C + TiO₂) where the Pd nanoparticles were reduced in the physical mixture of carbon and TiO₂ and Pd/TiO₂-C where the Pd nanoparticles were reduced firstly in TiO₂ and the carbon was inserted after. Pd/C was also inserted for comparison

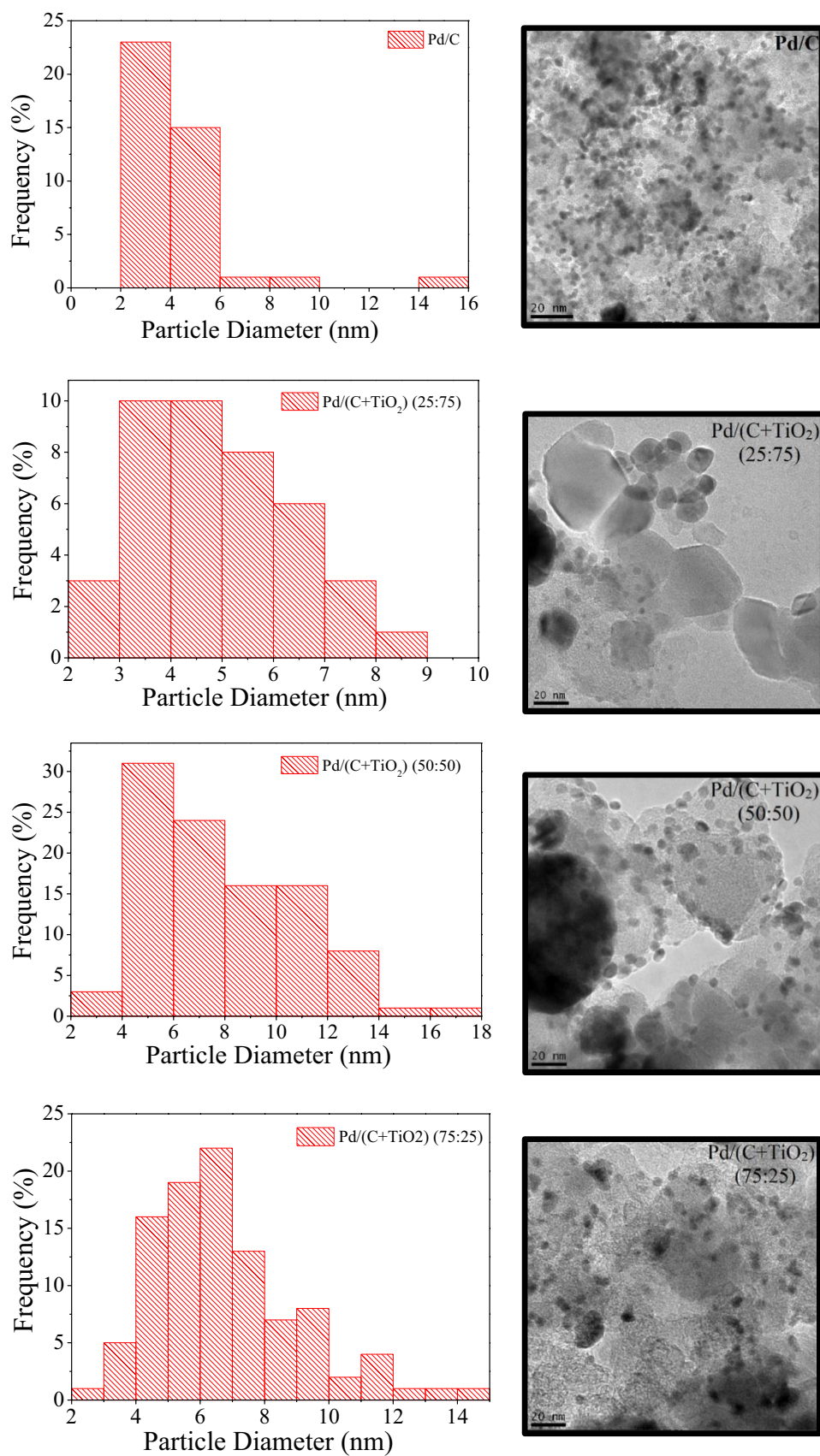
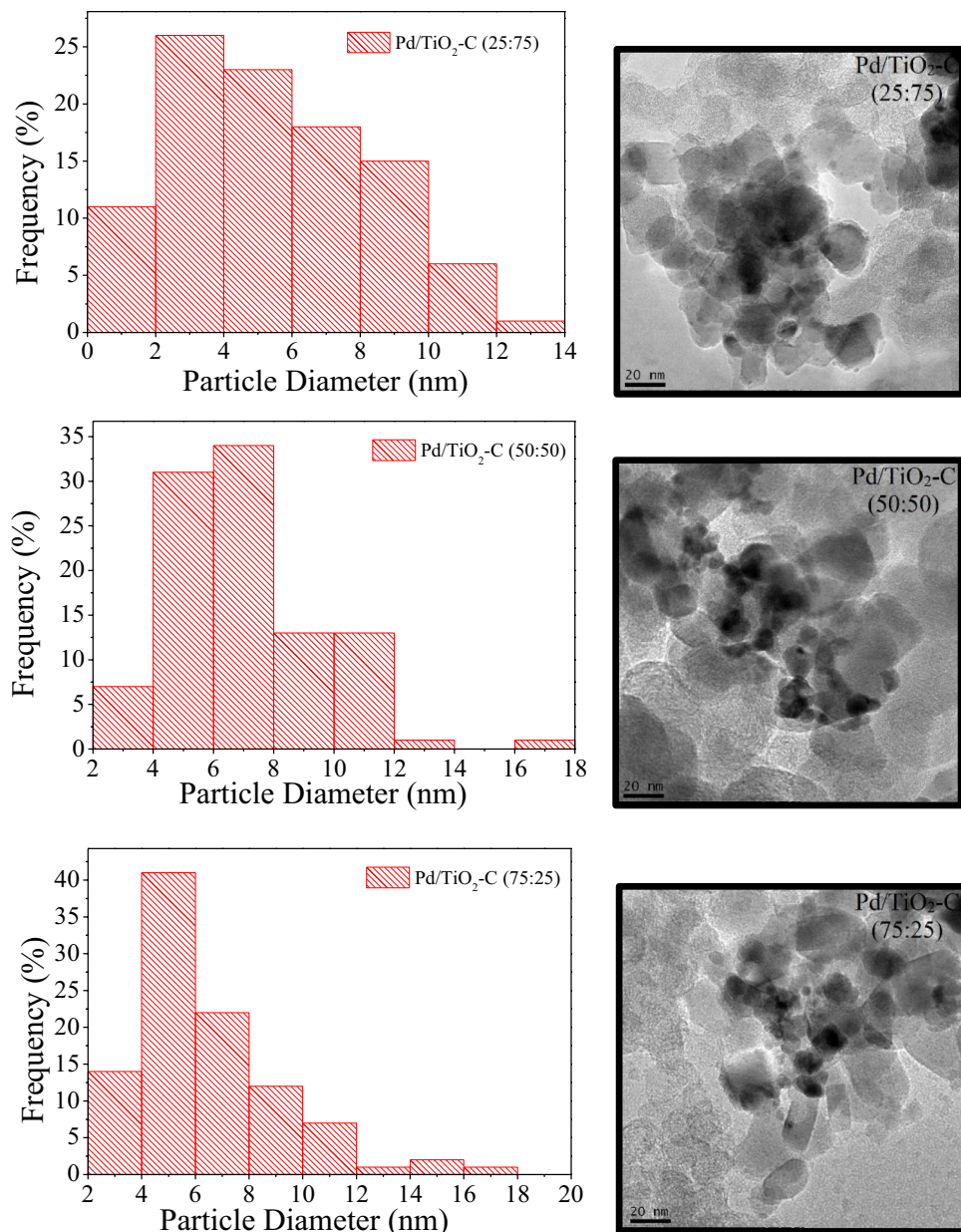


Fig. 1 (continued)

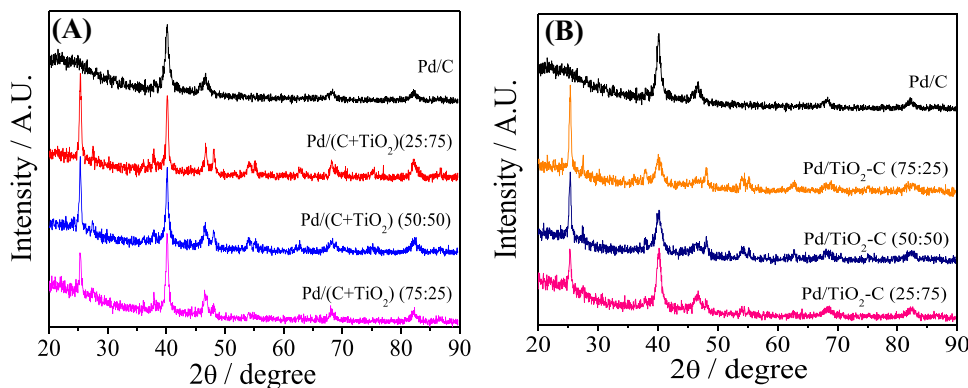
Electrochemical Characterizations (Half-Cell)

EIS was employed to further study the electrochemical properties of the electrocatalysts. Figure 3 presents the Nyquist (Fig. 3A and B) and Bode (Fig. 3C–F) diagrams obtained. The spectra of all electrocatalysts correspond to a simple Randles circuit, modified to incorporate the infinite diffusion related to Warburg impedance ($[R([RW]Q)]$). The data of each circuit is available in Table 2, where R_S is the solution resistance, R_{CT} is the charge transfer resistance, Y_0 is the admittance term, which contains the diffusion coefficient information for the constant phase element (CPE) and the Warburg impedance (W); and n is the exponential value of the CPE expression.

From these diagrams and fitted values, some behaviors can be inferred: the Bode diagrams suggest hybrid capacitor and resistor behavior for this specific process. While all phase value maximums are lower than $\pi/2^\circ$, their presence at lower frequencies implies that some charge effects are in motion during this process. These charge effects, along with the relatively high n values, explain the loss of Nyquist plots' semi-circle definition.

The reduction of Pd in the C + TiO₂ mixture produced a material with a lower R_S value at the 50:50 ratio when compared to 25:75 and 75:25. Also, the difference between Pd/C and this material R_S is only $\sim 9.0 \Omega$, implying a very small impact on the double layer formation. This suggests that the addition of TiO₂ in the C support, by this method, greatly

Fig. 2 XRD patterns for **A** Pd/(C + TiO₂) and **B** Pd/TiO₂-C electrocatalysts



affects its surface charge distribution when one of the components is in excess, but not in the same proportions. Interestingly, the effect observed for the other method is the opposite, as the direct deposition of Pd on TiO₂ and further addition of C at the same proportion resulted in a significant increase in the R_S , while modestly increasing the R_S in other distributions. As previously discussed, this could be the effect of the lower electronic conductivity of TiO₂, and its inefficiency to produce active sites for PdNPs. Among all electrocatalysts, both Pd/(C + TiO₂) (50:50) and Pd/TiO₂-C (50:50) presented lower R_{CT} values (0.956 and 1.49 kΩ, respectively), a decrease of ~54 and ~29% when compared to Pd/C. This not only suggests that the addition of TiO₂ to the system is beneficial but also suggests that the predominant structure produced by the mixture method is considerably more conductive than the direct addition of Pd on TiO₂.

The n exponential value of the CPE expression is mathematically correlated to the roughness of the surface affecting the double electric layer formation, and it is close to 1.0 for completely smooth surfaces, such as pure metallic electrodes, with a decrease of this value as the roughness increases [39, 40]. The Pd/(C + TiO₂) (50:50) and Pd/TiO₂-C (75:25) presented a high n value when compared to all other electrocatalysts. This suggests that these materials, when

cast on the electrodes, presented greater exposure or better distribution of the metals on the surface. This could be beneficial due to the increase in catalytic sites. Therefore, it could be expected that the Pd/(C + TiO₂) (50:50), Pd/TiO₂-C (75:25), and Pd/TiO₂-C (50:50) could present optimal performance in the half-cell analyses, due to their lower R_{CT} and/or greater metallic surface behavior.

Electrochemical properties and catalytic activities of the prepared electrocatalysts were evaluated using cyclic voltammetry. Figure 4 shows the cyclic voltammograms of both batches in 2.0 mol L⁻¹ KOH. Pd/C was also inserted for comparison. From this figure, it is possible to observe that the CVs are much similar, indicating that the introduction of TiO₂ has just little effect on the Pd profile [36]. It is also possible to observe peaks associated with hydrogen desorption/adsorption around -0.7 and -0.8 V, respectively. In the forward scan and at ~-0.3 V, there is a peak associated with the formation of the palladium (II) oxide and, in the cathodic sweep, another peak at about -0.3 V, associated with the reduction of Pd oxide to Pd [41, 42]. For both batches, Pd/C showed the highest area, which could be attributed to the lower TiO₂ electric conductivity and surface area [32].

Figure 5 presents the voltammetric pattern featuring the electro-oxidation of formate in alkaline media, which is characterized by two peaks. According to Noborikawa et al. [43], in the forward scan, there is a current increase until a point that the surface deactivates, which is caused by the oxide coverage. Besides, in the reverse scan, the surface oxides are reduced and the surface reactivates. Analyzing this figure, it is possible to affirm that all prepared materials are better than just Pd/C for formate electro-oxidation since they showed higher current densities when compared to Pd/C. However, among the materials in the study, Pd/(C + TiO₂) (50:50) and Pd/TiO₂-C (75:25) showed the highest currents toward formate oxidation, in agreement with the EIS analyses.

Many authors have indicated that oxide supports such as TiO₂ promote the oxidation of the poisoning intermediaries through the bifunctional mechanism while others attributed the higher catalytic activity in terms of metal reactivity

Table 1 Mean crystallite size obtained from XRD measurements and mean nanoparticle size obtained by TEM images

Electrocatalysts	Mean crystallite size (XRD) nm	Mean nanoparticle size (TEM) nm
Pd/C	6.0	3.7
Pd/(C + TiO ₂) (25:75)	6.4	5.5
Pd/(C + TiO ₂) (50:50)	7.5	7.9
Pd/(C + TiO ₂) (75:25)	7.0	6.7
Pd/TiO ₂ -C (75:25)	3.6	5.4
Pd/TiO ₂ -C (50:50)	7.6	7.2
Pd/TiO ₂ -C (25:75)	4.9	6.4

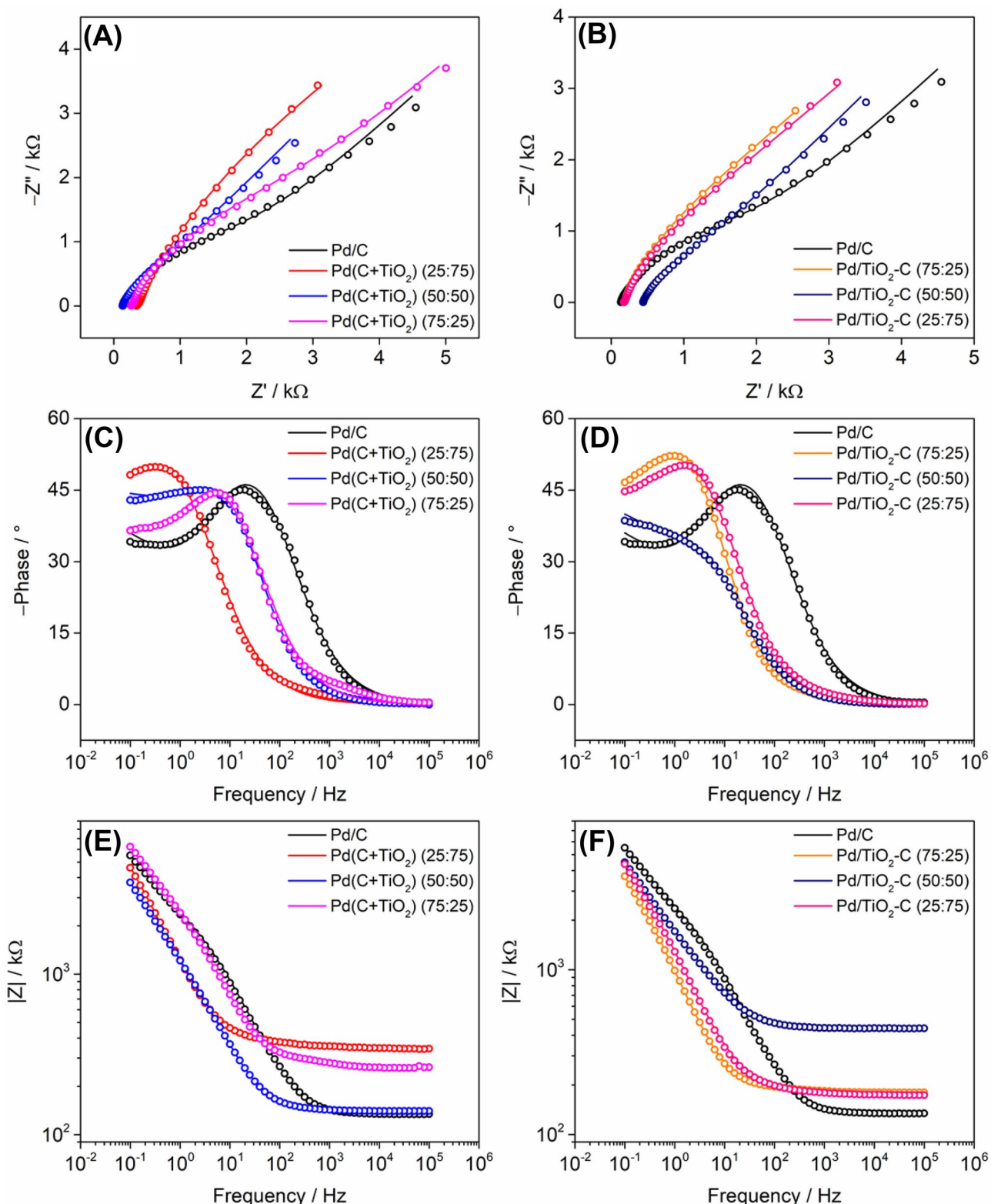


Fig. 3 Nyquist diagrams of Pd/C and **A** $\text{Pd}(\text{C}+\text{TiO}_2)$ electrocatalysts; and **B** $\text{Pd/TiO}_2\text{-C}$ electrocatalysts, in presence of $1.0 \text{ mmol L}^{-1} [\text{Fe}(\text{CN}_6)]^{3-/4-}$, in $0.1 \text{ mol L}^{-1} \text{ KCl}$. $E=200 \text{ mV}$; Bode diagrams

of **C** and **E** $\text{Pd}(\text{C}+\text{TiO}_2)$ and **D** and **F** $\text{Pd/TiO}_2\text{-C}$, in presence of $1.0 \text{ mmol L}^{-1} [\text{Fe}(\text{CN}_6)]^{3-/4-}$, in $0.1 \text{ mol L}^{-1} \text{ KCl}$. $E=200 \text{ mV}$

Table 2 Data obtained by $[R([RW]Q)]$ equivalent circuit

Electrocatalysts	R_S (Ω)	R_{CT} ($k\Omega$)	CPE	Warburg impedance
Pd/C	131	2.090	$Y_0=41.3 \mu\text{S s}^n$ $n=0.757$	$Y_0=273 \mu\text{S} \sqrt{s}$
Pd/(C+TiO ₂) (25:75)	351	10.30	$Y_0=246 \mu\text{S s}^n$ $n=0.737$	$Y_0=305 \mu\text{S} \sqrt{s}$
Pd/(C+TiO ₂) (50:50)	140	0.9560	$Y_0=108 \mu\text{S s}^n$ $n=0.815$	$Y_0=320 \mu\text{S} \sqrt{s}$
Pd/(C+TiO ₂) (75:25)	266	3.170	$Y_0=68.1 \mu\text{S s}^n$ $n=0.761$	$Y_0=243 \mu\text{S} \sqrt{s}$
Pd/TiO ₂ -C (75:25)	182	3.020	$Y_0=220 \mu\text{S s}^n$ $n=0.816$	$Y_0=331 \mu\text{S} \sqrt{s}$
Pd/TiO ₂ -C (50:50)	439	1.490	$Y_0=104 \mu\text{S s}^n$ $n=0.745$	$Y_0=277 \mu\text{S} \sqrt{s}$
Pd/TiO ₂ -C (25:75)	180	3.650	$Y_0=174 \mu\text{S s}^n$ $n=0.765$	$Y_0=282 \mu\text{S} \sqrt{s}$

variation due to electronic interactions between noble metals and TiO₂ [44–46]. It has been observed that the adsorption of a water molecule on TiO₂ favors its dissociation, resulting in Ti-OH groups [24, 28] which could contribute to the enhanced activity of TiO₂ content catalysts.

In Antolini reviews [24], considering methanol oxidation on Pt-TiO₂, it was found that in presence of TiO₂, the electron transfer rate of methanol oxidation accelerated. Thus, the interaction between platinum active sites and the metal oxide could enhance the charge transfer at the interface but an excessive amount of TiO₂ could block some platinum active sites, decreasing the electrical conductivity of the catalyst. Moreover, the enhanced methanol oxidation reaction activity of Pt in the presence of TiO₂ has been attributed to both the bifunctional mechanism and the electronic effect.

Wang et al. [47] affirm that formate adsorbs on the Pd surface forms the stable intermediate species, HCO*O* (where the asterisks represent chemisorption to the surface). At room temperature, HCO*O* was slowly converted into HCOO* which is a reactive specie and thus, it rapidly formed hydride on the Pd surface and CO₂ was then released. According to some authors [48, 49], HCO*O* could act as a poisoning

specie blocking the active Pd sites, and consequently, the catalytic activity toward formate oxidation could be increased by reducing the energy of the Pd–O bond, which in turn will lower the activation energy for the conversion of HCO*O* into HCOO* species.

According to Bai et al. [50], the formate oxidation reaction (FOR) on the Pd/C electrode undergoes a series of reactions in an alkaline medium, including $\text{HCOO}_{\text{ad}}^- \rightarrow \text{H}_{\text{ad}}$. Furthermore, they affirm that weak adsorption of $\text{HCOO}_{\text{ad}}^-$ facilitates the FOR and the FOR activity of catalysts also relates to OH_{ad}^- species, since the enhanced interaction between H_{ad} and OH_{ad}^- species also makes a special contribution to FOR activity enhancement. Choun et al. [51] report that H_{ad} species produced during the oxidation of HCOO^- is the important intermediate species since high coverage of H_{ad} inhibits the HCOO^- adsorption onto Pd surfaces, causing slow oxidation kinetics of HCOO^- .

Hence, according to several studies [51–55], decreasing the chemisorption strength of adsorbed species by modifying the electronic structure of Pd can contribute to an enhancement in the catalytic activity. Therefore, the best results obtained using TiO₂ as support could be attributed to the

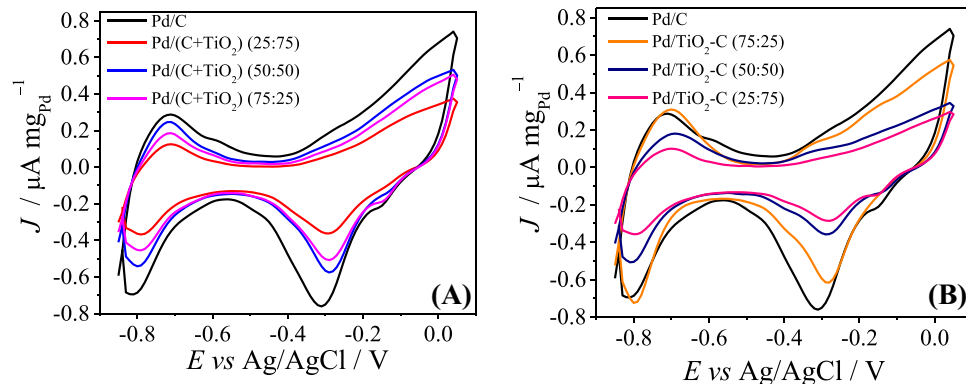
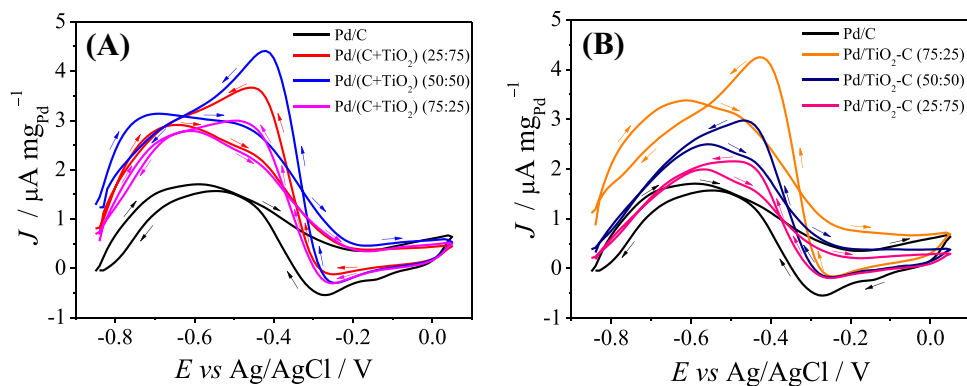
Fig. 4 Cyclic voltammograms in 2.0 mol L⁻¹ KOH at $v = 10 \text{ mV s}^{-1}$ for **A** Pd/(C+TiO₂) and **B** Pd/TiO₂-C electrocatalysts

Fig. 5 Cyclic voltammograms in $2.0 \text{ mol L}^{-1} \text{ KOH} + 0.02 \text{ mol L}^{-1}$ potassium formate at $\nu = 10 \text{ mV s}^{-1}$ for **A** Pd/(C + TiO₂) and **B** Pd/TiO₂-C electrocatalysts



presence of Ti–OH surface groups, and/or the oxidation of the poisoning intermediaries through the bifunctional mechanism, and/or the electronic interactions between Pd and TiO₂.

The stability of the electrocatalysts was evaluated through CA at a fixed potential, shown in Fig. 6. As observed in the CV in presence of formate, all TiO₂ content electrocatalysts showed higher currents than Pd/C, indicating the activity of TiO₂ toward formate electro-oxidation. Moreover, the catalysts with TiO₂ content also showed the highest stability.

Pd/TiO₂-C (75:25) showed higher current values compared to other prepared electrocatalysts; however, Pd/TiO₂-C (25:75) showed similar performance in comparison with Pd/C. All Pd/(C + TiO₂) showed higher current values compared with Pd/C; these results confirmed that the activity of the prepared electrocatalysts is dependent on the preparation method, but not entirely on the actual active area values at room temperature.

Fuel Cell Measurements (Single Cell)

Single-cell tests were performed to confirm the best activity of TiO₂ content electrocatalysts in the direct formate fuel cell. Figure 7 shows the cell potential and power density curves for all prepared electrocatalysts and the summarized results are available in Table 3, showing open circuit potential (OCV) and maximum power density (MPD).

In contrast to the electrochemical measurements, all materials prepared to reduce the Pd on the TiO₂ (Pd/TiO₂-C) showed maximum power densities lower than Pd/C, showing that these materials were not efficient in a single-cell environment. Nevertheless, the materials in which the Pd was reduced on the physical mixture of carbon and TiO₂, Pd/(C + TiO₂) showed better power densities when compared to Pd/C, except the Pd/(C + TiO₂) (25:75), in which the TiO₂ is in the major proportion.

According to Ahadi et al. [56], studying the conductivity in Pt/C electrocatalysts, the only components of a catalytic layer (CL) that could conduct electrons are C and Pt particles. On the other hand, the Pt particles have shown a small volume fraction when compared to C particles. Thus, the electron conduction in CL should be determined by the properties of the carbon phase. It is known that carbon supports are electronically conductive and that carbon surface area provides the active sites for Pt nanoparticles [19, 57] while, due to the low d-band mobility, TiO₂ shows low electrical conductivity [58].

Matos et al. [26] studied the effect of TiO₂-C as support and evaluated also the effect of Pd supported on non-conductive support (Pd/SiO₂) and observed that the lack of the conductivity of the Pd/SiO₂ could be explained by the fact that Pd nanoparticles were fixed on non-conductive support. This information could explain the worst efficiency

Fig. 6 Chronoamperometric measurements at $-0.55 \text{ V vs Ag/AgCl/KCl}$ (3.0 mol L^{-1}) in $2.0 \text{ mol L}^{-1} \text{ KOH} + 0.02 \text{ mol L}^{-1}$ potassium formate for **A** Pd/(C + TiO₂) and **B** Pd/TiO₂-C electrocatalysts

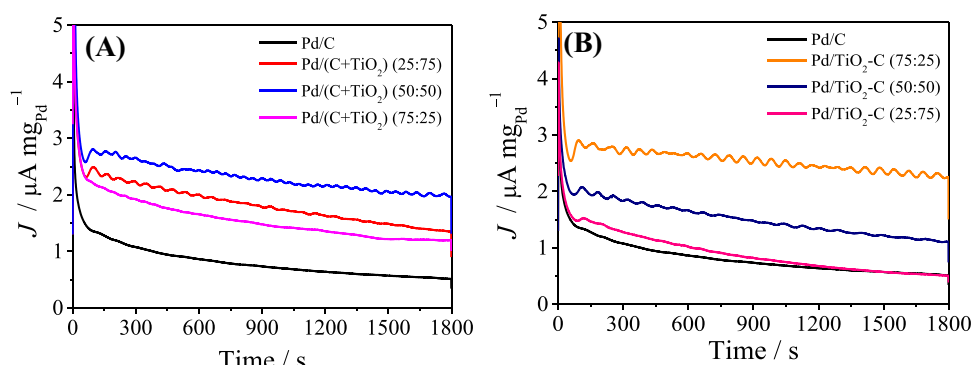


Fig. 7 Power density and polarization curves of a 5 cm^2 direct formate fuel cell at 60°C using $1.0\text{ mol L}^{-1}\text{ HCOONa} + 2.0\text{ mol L}^{-1}\text{ NaOH}$ for **A** Pd/(C + TiO₂) and **B** Pd/TiO₂-C electrocatalysts

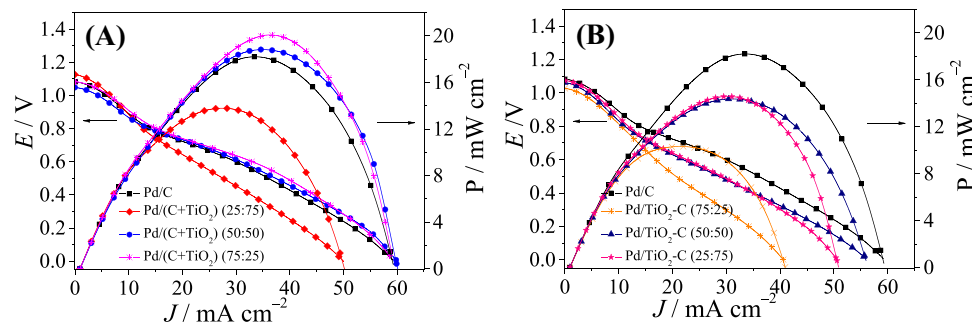


Table 3 Direct formate fuel cell results

Electrocatalysts	MPD mW cm^{-2}	Current density mA cm^{-2}	OCP V
Pd/C	18.2	59.2	1.08
Pd/(C + TiO ₂) (25:75)	13.8	50.4	1.13
Pd/(C + TiO ₂) (50:50)	18.8	60.1	1.05
Pd/(C + TiO ₂) (75:25)	20.1	58.9	1.08
Pd/TiO ₂ -C (75:25)	10.3	40.9	1.03
Pd/TiO ₂ -C (50:50)	14.4	55.9	1.06
Pd/TiO ₂ -C (25:75)	14.6	50.7	1.07

in single-cell experiments using Pd/TiO₂-C electrocatalysts; once in these materials, the PdNPs were firstly reduced on TiO₂, which shows lower conductivity than carbon. As rutile and anatase are semiconductors, their conductivity may not be sufficient for a fuel cell application, which was not observed in CV results.

Besides, it is also known that the nature of the chosen support can modify the electronic structure of the active sites, leading to an improvement in its efficiency [57] and that the number of active sites, with OH species adsorbed, is increased by the addition of TiO₂ and has particular importance in the fuel oxidation [49, 59, 60], what was observed with Pd/(C + TiO₂) electrocatalysts, except for the Pd/(C + TiO₂) (25:75), once, as already observed before [24], an excessive amount of TiO₂ could block some active sites, decreasing the electrical conductivity of the catalyst.

Conclusions

Here, we report the effect of TiO₂ as support along with carbon, and also the synthesis strategies (by preparing two batches of electrocatalysts: Pd/(C + TiO₂) and Pd/TiO₂-C) toward formate electro-oxidation in alkaline media. The Pd/(C + TiO₂) electrocatalysts showed better results when compared to Pd/C, being the Pd/(C + TiO₂) (75:25) the best material achieved in fuel cell experiments which were justified by the higher content of carbon black which shows good

electrical conductivity associated with small quantities of TiO₂ which works as co-catalyst on fuel oxidation, considering the bifunctional mechanism and/or metal reactivity variation due to electronic interactions between Pd and TiO₂.

Acknowledgements The authors wish to thank Instituto de Pesquisa Energéticas e Nucleares by TEM measurements, Centro Nacional de Pesquisa em Energia e Materiais (CNPEM), and LNNano for XRD analysis. The authors are also grateful to Evonik Degussa Brasil Ltda and Cabot Corporation for TiO₂ and Vulcan Carbon samples.

Funding This study was financially supported by the Conselho Nacional de Desenvolvimento Científico e Tecnológico – CNPq (407674/2016-0; 408430/2016-8; 169966/2017-8, 405546/2018-1; 103085/2019-0, and 403961/2021-1), Fundação de Amparo à Pesquisa do Estado de São Paulo – FAPESP (2017/21097-3, 2019/23342-0 and 2020/01050-5), and the Coordenação de Aperfeiçoamento de Pessoal de Nível Superior—Brasil – CAPES, Finance Code 001, 88887.504861/2020-00.

Declarations

Conflict of Interest The authors declare no competing interests.

References

1. J. Goldemberg, Energy Policy (2006). <https://doi.org/10.1016/j.enpol.2005.03.009>
2. X.D. Wu, J.L. Guo, X. Ji, G.Q. Chen, Energy Policy (2019). <https://doi.org/10.1016/j.enpol.2018.12.005>
3. M.A. Hannan, M.S.H. Lipu, P.J. Ker, R.A. Begum, V.G. Agelidis, F. Blaabjerg, App. Energy (2019). <https://doi.org/10.1016/j.apenergy.2019.113404>
4. M. Child, O. Koskinen, L. Linnanen, C. Breyer, Renew. Sustain. Energy Rev. (2018). <https://doi.org/10.1016/j.rser.2018.03.079>
5. J.L. Aleixandre-Tudó, L. Castelló-Cogollos, J.L. Aleixandre, R. Aleixandre-Benavent, Renew. Energy (2019). <https://doi.org/10.1016/j.renene.2019.02.079>
6. A. Arshad, H.M. Ali, A. Habib, M.A. Bashir, M. Jabbal, Y. Yan, Therm. Sci. Eng. Prog. (2019). <https://doi.org/10.1016/j.tsep.2018.12.008>
7. R.A. Barreto, Econ. Model. (2018). <https://doi.org/10.1016/j.econmod.2018.06.019>
8. N. Edomah, Energy Rep. (2016). <https://doi.org/10.1016/j.egyr.2016.01.004>
9. M.V. Moreira, G.E. da Silva, Renew. Energy (2009). <https://doi.org/10.1016/j.renene.2009.01.002>

10. B.C. Ong, S.K. Kamarudin, S. Basri, Int. J. Hydrog. Energy (2017). <https://doi.org/10.1016/j.ijhydene.2017.01.117>
11. H.Q. Pham, T.T. Huynh, T.M. Pham, V.T.T. Ho, Int. J. Hydrog. Energy (2021). <https://doi.org/10.1016/j.ijhydene.2020.08.278>
12. D. Ye, Q. Lan, Q. Liao, Y. Yang, R. Chen, S. Wang, Z. Liu, X. Zhu, Carbon (2022). <https://doi.org/10.1016/j.carbon.2022.02.053>
13. O.C. Esan, X. Shi, Y. Dai, L. An, T.S. Zhao, Appl. Energy (2022). <https://doi.org/10.1016/j.apenergy.2022.118677>
14. E. Berretti, M.V. Pagliaro, A. Giaccherini, G. Montegrossi, F. Di Benedetto, G.O. Lepore, F. D'Acapito, F. Vizza, A. Lavacchi, Electrochim. Acta (2022). <https://doi.org/10.1016/j.electacta.2022.140351>
15. X. Sun, Y. Li, Int. J. Hydrog. Energy (2019). <https://doi.org/10.1016/j.ijhydene.2019.01.240>
16. A.O. Santos, J.C.M. Silva, R.M. Antoniassi, E.A. Ponzio, O.C. Alves, Int. J. Hydrog. Energy (2020). <https://doi.org/10.1016/j.ijhydene.2020.08.165>
17. S. Luo, Y. Wang, T.C. Kong, W. Pan, X. Zhao, D.Y.C. Leung, J. Power Sources (2021). <https://doi.org/10.1016/j.jpowsour.2021.229526>
18. A.M. Bartrom, J.L. Haan, J. Power Sources (2012). <https://doi.org/10.1016/j.jpowsour.2012.04.032>
19. R. Bock, H. Karoliussen, B.G. Pollet, M. Secanell, F. Seland, D. Stanier, O.S. Burheim, Int. J. Hydrog. Energy (2018). <https://doi.org/10.1016/j.ijhydene.2018.10.221>
20. L. Lan, J. Li, Y. Yang, L. Zhang, L. Zhang, Q. Fu, X. Zhu, Q. Liao, Carbon (2022). <https://doi.org/10.1016/j.carbon.2021.12.071>
21. L. An, R. Chen, J. Power Sources (2016). <https://doi.org/10.1016/j.jpowsour.2016.04.082>
22. J. Liu, H.J. Choi, L.-Y. Meng, J. Ind. Eng. Chem. (2018). <https://doi.org/10.1016/j.jiec.2018.02.021>
23. M.T. Anwar, X. Yan, S. Shen, N. Husnain, F. Zhu, L. Luo, J. Zhang, Int. J. Hydrog. Energy (2017). <https://doi.org/10.1016/j.ijhydene.2017.10.152>
24. E. Antolini, Appl. Catal. B: Environ. (2018). <https://doi.org/10.1016/j.apcatb.2018.06.029>
25. A.S. Bandarenka, M.T.M. Koper, J. Catal. (2013). <https://doi.org/10.1016/j.jcat.2013.05.006>
26. J. Matos, A. Borodzinski, A.M. Zychora, P. Kedzierzawski, B. Mierza, K. Juchniewicz, M. Mazurkiewicz, J.C. Hernández-Garrido, Appl. Catal. B Environ. (2015). <https://doi.org/10.1016/j.apcatb.2014.07.063>
27. S.-Y. Huang, P. Ganeshan, B.N. Popov, Appl. Catal. B: Environ. (2011). <https://doi.org/10.1016/j.apcatb.2010.11.026>
28. Y. Wang, J. Wang, G. Han, C. Du, Y. Sun, L. Du, M. An, G. Yin, Y. Gao, Y. Song, Appl. Surf. Sci. (2019). <https://doi.org/10.1016/j.apsusc.2018.12.211>
29. S. Samad, K.S. Loh, W.Y. Wong, T.K. Lee, J. Sunarso, S.T. Chong, W.R. Wan Daud, Int. J. Hydrog. Energy. (2018). <https://doi.org/10.1016/j.ijhydene.2018.02.154>
30. P. Sabatier, Ber. Dtsch. Chem. Ges. (1911). <https://doi.org/10.1002/cber.19110440303>
31. A. Vittadini, A. Selloni, F.P. Rotzinger, M. Grätzel, Phys. Rev. Lett. (1998). <https://doi.org/10.1103/PhysRevLett.81.2954>
32. Q. Lv, M. Yin, X. Zhao, C. Li, C. Liu, W. Xing, J. Power Sources (2012). <https://doi.org/10.1016/j.jpowsour.2012.06.051>
33. S.G. da Silva, J.C.M. Silva, G.S. Buzzo, R.F.B. De Souza, E.V. Spinacé, A.O. Neto, M.H.M.T. Assumpção, Int. J. Hydrog. Energy (2014). <https://doi.org/10.1016/j.ijhydene.2014.04.169>
34. J.C.M. Silva, M.H.M.T. Assumpção, P. Hammer, A.O. Neto, E.V. Spinacé, E.A. Baranova, ChemElectroChem (2017). <https://doi.org/10.1002/celec.201600701>
35. M.H.M.T. Assumpção, S.G. da Silva, R.F.B. De Souza, G.S. Buzzo, E.V. Spinacé, M.C. Santos, A.O. Neto, J.C.M. Silva, J. Power Sources (2014). <https://doi.org/10.1016/j.jpowsour.2014.06.025>
36. Y. Song, C. Wei, X. Zhang, X. Wei, X. Song, Z. Sun, Mat. Chem. Phys. (2015). <https://doi.org/10.1016/j.matchemphys.2015.05.030>
37. W.-L. Qu, Z.-B. Wang, Y. Gao, C. Deng, R.-H. Wang, L. Zhao, X.-L. Sui, Int. J. Hydrog. Energy (2018). <https://doi.org/10.1016/j.ijhydene.2017.11.046>
38. C. Wang, X. Cai, Y. Chen, Z. Cheng, X. Luo, S. Mo, L. Jia, P. Lin, Z. Yang, Chem. Eng. J. (2017). <https://doi.org/10.1016/j.cej.2017.02.033>
39. A. Lasia, Electrochemical impedance spectroscopy and its applications, in: Modern aspects of electrochemistry (Springer, 2002) pp. 143–248
40. A.R.C. Bredar, A.L. Chown, A.R. Burton, B.H. Farnum, ACS Appl. Energy Mat. (2020)
41. Y.-H. Qin, Y. Zhuang, R.-L. Lv, T.-L. Wang, W.-G. Wang, C.-W. Wang, Electrochim. Acta (2015). <https://doi.org/10.1016/j.electacta.2014.12.050>
42. F. Zhang, D. Zhou, M. Zhou, J. Energy Chem. (2016). <https://doi.org/10.1016/j.jecchem.2015.10.013>
43. J. Noborikawa, J. Lau, J. Ta, S. Hu, L. Scudiero, S. Derakhshan, S. Ha, J.L. Haan, Electrochim. Acta (2014). <https://doi.org/10.1016/j.electacta.2014.04.188>
44. A.E. Alvarez, A.N. Gravina, J.M. Sieben, P.V. Messina, M.M.E. Duarte, Mat. Sci. Eng.: B (2016). <https://doi.org/10.1016/j.mseb.2016.05.017>
45. C.-S. Chen, F.-M. Pan, Appl. Catal. B: Environ. (2009). <https://doi.org/10.1016/j.apcatb.2009.07.008>
46. N. Rajalakshmi, N. Lakshmi, K.S. Dhathathreyan, Int. J. Hydrog. Energy (2008). <https://doi.org/10.1016/j.ijhydene.2008.09.032>
47. W.J. Wang, S. Hwang, T. Kim, S. Ha, L. Scudiero, Electrochim. Acta (2021). <https://doi.org/10.1016/j.electacta.2021.138531>
48. J.T. Gray, S.W. Kang, J.-I. Yang, N. Kruse, J.-S. McEwen, J.C. Park, S. Ha, Appl. Catal. B: Environ. (2020). <https://doi.org/10.1016/j.apcatb.2019.118478>
49. J. Shim, C.-R. Lee, H.-K. Lee, J.-S. Lee, E.J. Cairns, J. Power Sources (2001). [https://doi.org/10.1016/S0378-7753\(01\)00817-5](https://doi.org/10.1016/S0378-7753(01)00817-5)
50. J. Bai, Q. Xue, Y. Zhao, J.-X. Jiang, J.-H. Zeng, S.-B. Yin, Y. Chen, A.C.S. Sustain, Chem. Eng. (2019). <https://doi.org/10.1021/acssuschemeng.8b06193>
51. M. Choun, K. Ham, D. Shin, J.K. Lee, J. Lee, Catal. Today (2017). <https://doi.org/10.1016/j.cattod.2017.04.026>
52. S. Hong, S. Chung, J. Park, J.P. Hwang, C.H. Lee, S. Uhm, S. Bong, J. Lee, ACS Catal. (2021). <https://doi.org/10.1021/acscatal.0c03555>
53. J. Jiang, A. Wieckowski, Electrochim. Commun. (2012). <https://doi.org/10.1016/j.elecom.2012.02.017>
54. T. Takamura, F. Mochimaru, Electrochim. Acta (1969). [https://doi.org/10.1016/0013-4686\(69\)80008-3](https://doi.org/10.1016/0013-4686(69)80008-3)
55. M. Choun, S. Hong, J. Lee, J. Electrochem. Soc. (2018). <https://doi.org/10.1149/2.0341815jes>
56. M. Ahadi, M. Tam, J. Stumper, M. Bahrami, Int. J. Hydrog. Energy (2019). <https://doi.org/10.1016/j.ijhydene.2018.12.016>
57. G.R. Mirshekari, A.P. Shirvaniyan, J. Electroanal. Chem. (2019). <https://doi.org/10.1016/j.jelechem.2019.03.077>
58. G.D. Bhowmick, M.T. Noori, I. Das, B. Neethu, M.M. Ghangrekar, A. Mitra, Int. J. Hydrog. Energy (2018). <https://doi.org/10.1016/j.ijhydene.2018.02.188>
59. M. Kübler, T. Jurzinsky, D. Ziegenbalg, C. Cremers, J. Power Sources (2018). <https://doi.org/10.1016/j.jpowsour.2017.07.114>
60. M. Choun, J. Lee, J. Energy Chem. (2016). <https://doi.org/10.1016/j.jechem.2016.04.008>

Publisher's Note Springer Nature remains neutral with regard to jurisdictional claims in published maps and institutional affiliations.

Springer Nature or its licensor (e.g. a society or other partner) holds exclusive rights to this article under a publishing agreement with the author(s) or other rightsholder(s); author self-archiving of the accepted manuscript version of this article is solely governed by the terms of such publishing agreement and applicable law.